Nuclear Instruments and Methods in Physics Research B 100 (1995) 47–54

ELSEVIER

NIM B
Beam Interactions with Materials & Atoms

Measurement of negative-ion and -cluster sputtering with highly-charged heavy ions

G. Schiwietz [a,*], M. Briere [b], D. Schneider [b], J. McDonald [b], C. Cunningham [b]

[a] *Hahn–Meitner-Institut GmbH, Abteilung FD, Glienicker Str. 100, 14109 Berlin, Germany*
[b] *Lawrence Livermore National Laboratory, Livermore, CA 94550, USA*

Received 24 May 1994; revised form received 13 January 1995

Abstract

A single-detector technique for the measurement of negative ion time-of-flight spectra is introduced in this work. Spectra are presented for 390 keV Xe^{44+} ions at normal incidence on different samples. Mass distributions for C_n and Si_nO_m clusters indicate that highly charged ions lead to a statistical off-surface formation of heavy clusters, whereas low-energy singly-charged ions may directly produce heavy carbon clusters. The detection technique has proven to be very efficient and might even be used as a nearly non-destructive surface-analysis method for investigations of time dependent surface modifications.

1. Introduction

The ion-induced sputtering process has been investigated for one and a half century [1] and systematic studies of the projectile dependence started about one century ago [2]. The dependence of the total sputtering yield on the incident energy, dose and entrance angle of the (in most cases) singly charged projectile have been determined for a variety of projectile–target systems (for a review see Refs. [3,4]). The charge-state fractions, angular distributions and energy spectra of sputtered ions as well as the target-temperature dependence, have also been investigated [3,5–8]. The large body of experimental and theoretical works for singly charged projectiles suggests a distinction between (isolated) nuclear, thermal and electronic sputtering mechanisms. In the case of nuclear sputtering, a sequence of isolated (independent) binary atom–atom collisions leads to an ejection of (mainly) surface atoms [9–13]. Under this condition and some other model assumptions, such as the independence of the atom transport on the atom/surface distance, simple equations for the total as well as differential sputtering yields could be derived from the Boltzmann transport equation [12].

If the density of the collision cascades exceeds a certain limit, nearly all atoms in a volume element are set in motion and non-linear effects come into play. These so-called thermal spikes or collision spikes are found for heavy projectiles or molecular ions interacting with heavy target atoms at energies somewhat below the nuclear stopping power maximum [14,4]. Thermal spikes may simply be viewed as a local melting of the substrate. The corresponding phase transitions have been identified in molecular-dynamics simulations [15].

Contrarily, light projectiles (electrons, protons or even photons) may induce particle ejection via electronic processes (for a review on electronic desorption see Ref. [16]). Quite often, such electronic processes depend critically on details of the target structure [16] and especially for insulators strong non-linear effects at low doses have been found [4]. However, especially for highly charged incident ions non-linear electronic effects are expected to influence the sputtering yields [17,18], since the potential energy of these ions can exceed their kinetic energy and many electronic transition probabilities are expected to scale with the squared projectile charge. Only a few pioneering experiments have been performed with these ions and no consistent picture of the corresponding sputtering mechanisms has evolved so far [18–20].

In this work we describe an experimental technique that may be used to investigate mass spectra of negative ions and clusters (for a review on cluster sputtering see Ref. [21]). It is believed that such measurements are more sensitive to specific sputtering mechanisms than investigations of integral sputtering yields. Mass distributions for C_n and Si_nO_m clusters are presented and discussed with special emphasis on cluster production mechanisms.

* Corresponding author. Tel. +49 30 8062 2448, fax +49 30 8062 2097.

SSDI 0168-583X(95)00189-1

2. Experimental method

The aim of this work was to build up an ion mass-analyzer system that enables an efficient detection of sputtered ions and eventually could be used to investigate the initial velocity distribution of sputtered ions. Because highly-charged heavy ions shall be used in subsequent works, we have to deal with very low currents of incident ions.

For highly charged light ions, e.g. Ne^{10+}, or heavy ions at intermediate charge states, electron cyclotron-resonance (ECR) sources are probably the best choice. Similar charge state are also produced with recoil-ion sources, but the currents are quite low in this case. Slow heavy ions of the highest charge states may be extracted from an electron-beam ion trap (EBIT) [22]. Here we have to deal with low DC ion "currents" on the order of about 1000 ions per second (typically up to Xe^{50+} or U^{80+}). All results presented in this work have been obtained at the Livermore EBIT source.

Low-energy ions are mass analyzed usually with magnetic spectrometers, e.g. quadrupole mass-spectrometers, or time-of-flight (TOF) analyzers. We decided to build an ion time-of-flight analyzer, since this method combines high efficiency with simultaneous detection of different ionic species. Hence, this method is well suited for low ion currents. In the case of DC ion beams, however, a start signal is needed for the TOF analysis. This signal should be independent of the nature of the sputtering mechanisms and its detection probability should be as close as possible to unity. For this purpose we chose to use the bunch of electrons emitted when the incident ion penetrates the surface. It should be emphasized that this signal is very efficient, since low energy ions, e.g. 10 keV U^{70+}, lead to about 300 electrons [23] and high energy heavy ions can cause an ejection of even more than 1000 electrons per incident ion [24]. The statistical fluctuations of the electron multiplicity (number distribution) are small enough to ensure nearly 100% detection efficiency for this prompt pulse of emitted electrons. Furthermore, this signal should be independent of the specific scattering reactions of the incident ion and of the sputtering mechanisms involved. It is noted, that this would not be the case if we would use backscattered ions or emitted electrons due to ions of low charge state. We estimated that the lowest charge state where this method can safely be applied is about 5. In this work, however, O^{7+}-, Xe^{27+}-, Xe^{44+}- and U^{67+}-ions are used.

Fig. 1 shows a schematic view of the experimental setup used for the time-of-flight measurements. It consists basically of the target, an annular detector and an electrostatic field in between. The ion beam was focussed onto the target through the center holes of the annular detector and the acceleration grid. Thus, the measurements were all performed under normal incidence conditions. Negatively charged particles are accelerated towards the annular detector by a negative bias voltage applied to the target and the sample holder. A steering electrode (not shown in the

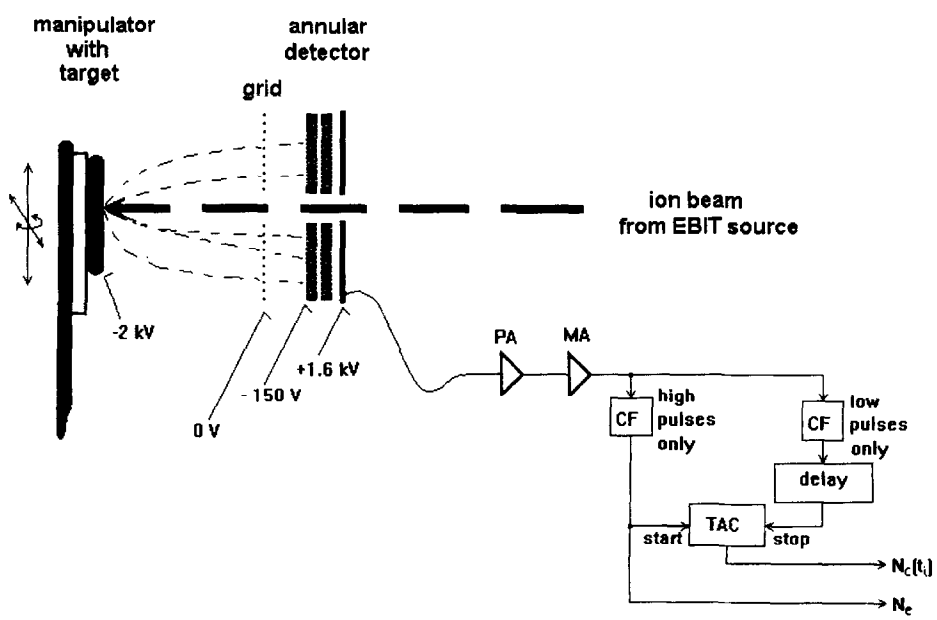

Fig. 1. Scheme of the experimental setup for the single-detector time-of-flight technique, showing the target mounted on a manipulator, the acceleration grid and the annular double-channel-plate detector. PA: preamplifier, MA: main amplifier, CF: constant-fraction discriminator, TAC: time-to-amplitude converter.

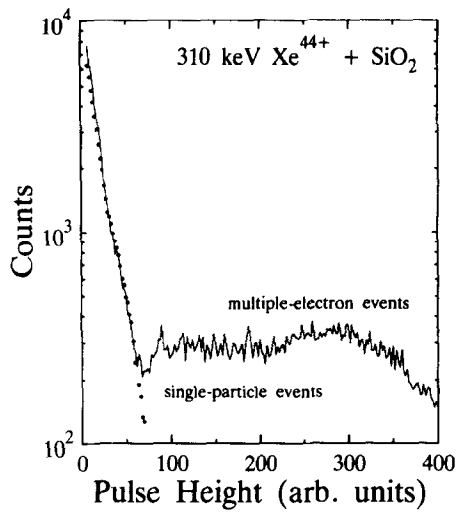

Fig. 2. Pulse-height spectrum of the annular detector for 310 keV $Xe^{44+} + SiO_2$ showing single-particle events from negative recoil ions and multiple-electron events induced by the incident ion (solid curve). Dotted curve: single-particle events due to an electron source.

figure) avoids focussing of particles into the center hole of the annular detector. The detector-entrance voltage of -150 V prevents secondary electrons produced at ground potential (in the beamline or at the grid) from being counted. The detector consists of two channelplates and an anode for fast pulse extraction. The rise time of the pulses is below 1 ns and this ensures good time resolution in the time-of-flight measurements. Before the single-detector technique for the measurement of ion time-of-flight spectra is explained in detail, the pulse height distribution of the annular detector for highly charged incident ions should be discussed.

Fig. 2 displays the pulse-height spectra of the annular detector for two different cases. The dotted curve is nearly exponentially decreasing and corresponds to single-particle events, namely electrons from an electron source. The solid curve was taken for Xe^{44+} ions incident on an oxidized Si sample. It corresponds to a superposition of single-particle events, in this case negative recoil ions, and a nearly flat part due to multiple-electron events induced by the incident ion. The pulse heights have been determined with a PC-based multichannel-analyzer system by using two slow main amplifiers (instead of one fast amplifier as in Fig. 1) and a linear-gate-and-stretcher in series. The mean pulse height of the flat part (extrapolated to zero) is about 15 times higher than the one associated with single-particle events (extrapolated to zero as well). Considering the detector efficiency, the grid transparancy and the size of the inactive inner region of the channelplates we estimate that about 30 electrons per incident ion are simultaneously focussed onto the channelplate detector. This result for 310 keV $Xe^{44+} + SiO_2$ may be compared with data by Kurz et al. [23] who determined an average number of 80 ejected electrons per incident ion for 300 keV Xe^{44+} + Au interactions. It is noted that our value corresponds to low-energy ejected electrons only, since for the spectra in Fig. 2 we have applied a target-bias voltage of only -300 V. Thus, electrons with energies above 5 eV may have perpendicular momentum components large enough to escape the detection. This, however, constitutes no problem for the ion time-of-flight measurements with a setup according to Fig. 1. The multiple-electron pulse even yields a fast and very efficient signal (about 95% of the ions lead to a high electron pulse) that is used as a start signal for our single-detector time-of-flight technique. Consequently, this pulse is also used for an accurate determination of the number of incident particles.

Some details of the electronic data acquisition system are given in the following. The pulses are extracted from the anode voltage via a capacitive coupling and fed into a preamplifier. The signal is further amplified using a fast main amplifier. The amplifier's signal output is connected to two constant-fraction discriminators of the same type with equal settings with respect to the timing. A necessary requirement for this experiment is that both discriminators need to have a lower as well as an upper level threshold, similar as single-channel analyzers. The lower level of one discriminator (the left CF in Fig. 1) is adjusted so that only high pulses can pass. This level corresponds to about channel 80 in Fig. 2. Thus, only if a multiple-electron event is detected a standard fast NIM output-signal is produced by this discriminator and triggers the time-to-amplitude converter. The stop input-signal of the time-to-amplitude converter comes via a delay box from the other constant-fraction discriminator. That discriminator accepts only low pulses corresponding to channels 5 to 70 in Fig. 2. Hence, this second discriminator is mainly sensitive to single-particle events as e.g. the detection of negative ions. As a result the time-to-amplitude converter is started by the fast electrons and stopped by the relatively slow negative ions that are both accelerated from the target into the same detector.

The electrons need less than 10 ns to arrive at the detector and thus yield a very stable timing signal. The expected uncertainty due to the energy distribution of ejected electrons is on the order of 1 ns. The ion time-of-flight depends on the mass-to-charge ratio, on the acceleration voltage and on the normal component of the initial velocity. Typical ion flight-times are on the order of 1 to 3 μs. The electronic time resolution was checked by using overlapping discriminator settings, e.g. a reduction of the lower level threshold of the left discriminator in Fig. 1 (corresponding to channel 50 or so). The measured line width was then below 1 ns. Thus, the time resolution that may be achieved using this technique is even good enough to obtain information on the initial energy distribution of sputtered ions.

3. First results and discussion

Absolute ion time-of-flight spectra, normalized per incident ion, may be deduced from the measured coincidence counts $N_c(t_i)$ for each channel of width Δt according to

$$dP/\,dt(t_i) = N_c(t_i)/(\Delta t\ \varepsilon_I N_e). \quad (1)$$

Here, N_e is the total number of multiple-electron counts and ε_I is the effective overall efficiency for the detection of negative ions. The ion detection efficiency and grid transparancy are known from previous experiments [25,26] yielding $\varepsilon_I = 0.55$ for low-energy ions (< 20 eV) and the setup used in this work. The effective detection efficiency for the multiple-electron pulses ε_e does not enter Eq. (1), since the count rates $N_c(t_i)$ as well as N_e are proportional to this quantity. However, from the spectrum in Fig. 2 one can determine a value of $\varepsilon_e = 0.93$ for Xe^{44+} projectiles and an extraction voltage of 300 V. For higher incident charge states and extraction voltages of 2 kV, as used for the measurements shown in Fig. 3, we expect ε_e to exceed 99%. It is emphasized that high values of ε_e allow for the use of low projectile currents and this goes hand in hand with a low background due to random coincidences.

Fig. 3 shows time-of-flight spectra for negative sputtered ions induced by 390-keV Xe^{44+} on SiO_2, Mo and graphite. All spectra were taken with a target-bias voltage of -2 kV and a constant background was subtracted from the spectra. The line at channel 70 corresponds to spurious coincidences due to differences in the pulse-height analysis of both constant-fraction discriminators (see Fig. 1). The intensity of this line was strongly dependent on the discriminator settings. The other lines are due to sputtered negative ions and clusters as these lines show up at a time-of-flight proportional to the square root of the target-bias voltage. It is seen that significant spectral components may be assigned to surface contaminations. Hydrogen and carbon contaminations have been found for all investigated target materials. The width of the hydrogen peaks for the three materials is about 10 ns and, hence, much larger than

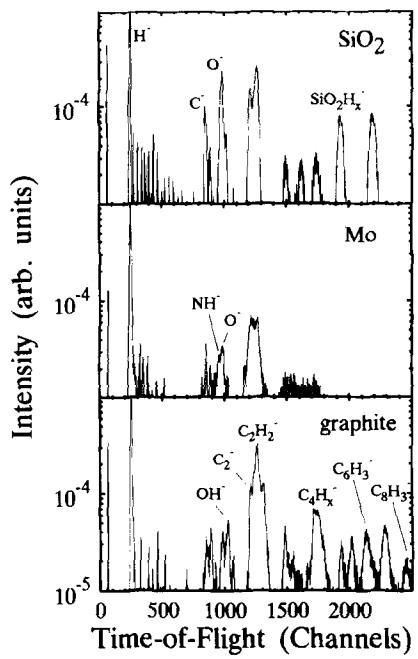

Fig. 3. Time-of-flight spectra of negative sputtered ions induced by 390 keV Xe^{44+} on different materials (SiO_2, Mo and graphite) after subtraction of a constant background.

the experimental time resolution. A closer examination shows that these peaks are asymmetric with a sharply decreasing tail on the right wing. This indicates, that the lines are influenced by the initial ion-velocity distributions.

Furthermore, negative clusters of the type $Si_lO_nH_m$ and C_nH_m with large values of l and n have been detected. The largest negative cluster that has been identified in this work is $C_{10}H_m$ with an intensity of about 1% of the dimer-like carbon clusters. C_nH_m clusters in the range of $50 < n < 80$ have also been detected, but individual lines could not be identified. For the graphite target we find enhanced $C_2H_2^-$, $C_4H_x^-$, $C_6H_3^-$ and $C_7H_3^-$ production in

Table 1
Negative carbon-cluster sputtering yields per ion Y^-_{Xe} and the corresponding kinetic energies $\bar{E}^-_{Xe}$ are displayed as a function of the cluster size n for 390 keV Xe^{44+} on a thick graphite sample. The yields represent the sum over the fractions containing different hydrogen contaminations and are subject to an uncertainty of about 40% on an absolute intensity scale. Also shown is the relative negative-cluster intensity Y^-_{vap} for vaporization of graphite at a temperature of 2400 K (taken from Ref. [28]) and the relative sputtering yield Y^-_{Cs} for 2.8 keV Cs projectiles (taken from Ref. [32]). The last two rows give electron affinities A for species of linear-chain type (taken from Ref. [31]) and estimated negative-charge-state fractions $f^-_{Xe,Cs}$ using the works of Refs. [33–35]

	$n=1$	$n=2$	$n=3$	$n=4$	$n=5$	$n=6$	$n=7$	$n=8$	$n=9$	$n=\infty$
$\bar{E}^-_{Xe}$ [eV]	3.1	2.3	1.6	1.8	–	–	–	–	–	–
Y^-_{Xe}	0.0020	0.0186	0.0022	0.0055	0.0010	0.0025	0.0026	0.00116	0.00033	–
Y^-_{Cs} [a]	0.0020	0.0063	0.00042	0.00068	0.00024	0.00034	0.00013	0.00016	–	–
$Y^-_{vap.}$ [a]	0.0020	7.14	0.0821	0.336	0.0279	0.0186	0.00164	0.0005	–	–
A [eV]	1.268	3.3	1.95	3.7	2.8	4.1	3.1	4.4	3.7	4.5
$f^-_{Xe,Cs}$	0.003 [b]	0.08	0.02	0.06	0.04	0.1	0.013	0.1	0.02	–

[a] Normalized to $Y^-_{Xe} = 0.002$ at $n = 1$.
[b] Obtained from the negative- and neutral-cluster yields of Ref. [32] (fitted to $n = 2$ to 4).

comparison to a small fraction of C^- and CH^-. Table 1 displays the corresponding carbon-cluster yields. The yield of clusters with a certain mass does not only depend on the production mechanisms (which are not understood in the case of highly charged incident projectiles). It also depends on the surface structure and on the cluster stability for a given geometry, charge state and degree of excitation [21]. Thus the electronic cluster structure has to be accounted for in the interpretation of the negative cluster yields. In the following we discuss different properties and mechanisms that determine the formation and stability of clusters.

A significant decomposition of large ($n > 6$) sputtered clusters with typical decay times on the order of 10 μs was observed in previous experiments [27]. Since this time scale agrees with our typical cluster flight-times, there might be indications of such a cluster decay in the TOF spectra. Except for the C_4H_m and C_6H_m clusters the right wings of the peaks in Fig. 3 do not show any shoulders that could correspond to reduced effective acceleration distances (decomposition). Furthermore, the relative cluster intensities for extraction voltages of 2 kV and 500 V, corresponding to different acceleration times, do not show systematic deviations. Hence, a decay of metastable clusters seems to play a minor role in our experiments.

In order to judge about the influence of the electronic cluster structure near the ground state on the cluster yield one may compare the present data with carbon cluster-abundances determined in evaporation experiments [28,29]. Results of such experiments [28] are also displayed in Table 1. Although the general trend of the evaporation data differs significantly from our data, it is evident that there is a pronounced odd/even oscillation of the cluster abundances independent of the production mechanism. Even numbers of carbon atoms are favoured, and this behaviour is also found for negative clusters containing more than 80 carbon atoms [29]. It is noted, that the reduced oscillation amplitude of our sputtering data is most likely due to an increased population of excited cluster states. Molecular-orbital calculations on the basis of a linear-combination-of-atomic-orbitals model have shown that the neutral-cluster distribution depends strongly on the temperature [30]. Furthermore, clusters with an even number of carbon atoms show much greater electron affinities than the odd species (see Table 1) [31]. This is due to half-filled bonding π-orbitals, which can be filled with an extra electron [30]. In the case of odd species the extra electron has to occupy an empty non-binding orbital. Thus, the odd/even oscillations are mainly caused by the oscillating electron affinity and reflect the quantum structure of the clusters. However, it has to be kept in mind that the graphite surface electron-affinity (work function) exceeds the affinities for all smaller clusters. Hence, the neutral-cluster fractions are expected to be much larger than the negative-charge fraction determined in this work.

If we exclude the production and transport of large clusters inside the bulk, their formation occurs near or at the surface. However, the importance of the different possible mechanisms that lead to formation of clusters is largely unsolved [21]. As will be discussed in the following, clusters may be formed

i) in multi-step processes, if the gas is in thermal equilibrium with the solid,

ii) due to direct production as an entity at the top-most layer, or

iii) via aggregation of atoms in front of the surface.

i) First of all it is emphasized that a temperature concept (thermal spike) seems not to be applicable to describe the present sputtering data. The evaporation results in Table 1 scaled by the temperature dependence of the C_n partial pressures [30] gave no satisfactory fits to our data, at least not for the tabulated temperatures up to 4000 K. Thus, the duration times for single sputtering events or the spatial extensions are to small to yield thermal equilibrium conditions. This is no surprise, since thermal spikes are not expected to be of any importance for light target materials such as carbon [11].

ii) Direct production of heavy clusters as a whole requires probably a long-range interaction (Coulomb interaction) between projectile and surface. Long-range interactions can cause a coherent excitation of those surface atoms that constitute the cluster. Such a mechanism is closely related to electronic desorption. It is, however, also conceivable that nuclear sputtering leads to ejection of larger compounds, where the mass spectrum is influenced by the microscopic surface topography.

In any case, the energy transfer Q to the cluster has to exceed the heat of sublimation $E_s(n)$ and the final kinetic energy E_{kin} is limited by

$$Q - E_s(n) > E_{kin} > Q - E_s(n) - E_d(n), \qquad (2)$$

where $E_d(n)$ is the dissociation energy of a cluster of size n. Thus, direct cluster production is expected to be determined by $E_s(n)$ and $E_d(n)$ and by a typical range associated with the ion–surface interaction. Hence, the relative mass distribution (not the total yield) should be nearly independent of the incident ion. First-order quantum mechanical perturbation theory for fast projectiles as well as adiabatic long-range dipole-excitation processes for slow projectiles and all processes that are determined by the microscopic surface topography are consistent with the above statement.

Considering that cross sections maximize at small energy transfers Q and that clusters with low kinetic energies are suppressed due to transmission through the (nearly planar) surface potential, we estimate $\bar{E}_{kin}(n)$ to be approximately $E_d(n)/2$ for $n > 1$. The mean kinetic energy of the monomer should then exceed the energy of all other clusters. These statements on the kinetic energy should also be valid for the statistical model discussed below.

iii) Some models assume that clusters are formed in front of the surface due to collisions between statistically

ejected atoms or small molecules [36,11,21]. If we assume a constant sticking probability P_s for each of these collisions, a quantitative analysis of the cluster yields $Y(n)$ is possible. This means we neglect the influence of the 6-dimensional phase-space distribution of sputtered atoms, cluster-size effects (constant fusion cross section), as well as the influence of the dissociation energy on P_s. For a large total sputtering yield $\bar{Y}$ one may also neglect fluctuations of the number of sputtered atoms and the mass distribution $Y(n)$ may be written as

$$Y(n) = \binom{\bar{Y}}{n} P_s^{(n-1)}(1-P_s)^{(\bar{Y}-n)} \quad \text{with } \bar{Y} = \sum_n nY(n). \tag{3}$$

This formula is similar to a binomial distribution (except for the lower boundary $n = 1$ and a constant factor P_s^{-1}) and for realistic parameters it leads to monotonic and rapidly decreasing yields as function of the cluster size. This trend is consistent with our Xe data as well as with the Cs data of Ref. [32], if we account for the influence of the electron affinity. The mean cluster size $\bar{n}$ may be obtained from Eq. (3) by using the fact that the binomial distribution is a probability distribution (normalized to unity):

$$\bar{n} = \frac{\bar{Y}}{\sum_n Y(n)} = \frac{P_s\bar{Y}}{1-(1-P_s)^{\bar{Y}}} \qquad \text{for } \bar{Y} \gg 1. \tag{4}$$

For small total sputtering yields $\bar{Y}$ we account for fluctuations on the order of $\pm\sqrt{\bar{Y}}$ and estimate

$$\bar{n} \approx 1 + \frac{P_s\bar{Y}}{2} \qquad \text{for } \bar{Y} \approx 1 \text{ and } P_s\bar{Y} \ll 1. \tag{5}$$

For the highly charged Xe projectiles we derive an experimental value of $\bar{n} = 2.5 \pm 0.5$ from Y_{Xe}^- and f_{Xe}^-. From previous works we estimate that in total about 6 carbon atoms are sputtered per incident Xe^{44+} ion [3]. The corresponding sticking probability calculated using Eq. (4) is $P_s = 0.4$, which is a realistic value. Using the same sticking probability (P_s is expected to be nearly independent on the projectile ion) and $\bar{Y}_{Cs} = 0.5$ [3], Eq. (5) predicts a mean cluster size of 1.10 ± 0.04 for singly charged Cs projectiles at 2.8 keV. From the corresponding experimental values [32] we derive $\bar{n}_{exp} = 1.31 \pm 0.05$.

The above estimates may serve as a guideline to distinguish between the two cluster-production mechanisms ii) (scattering as an entity) and iii) (statistical off-surface formation). First of all, the measured kinetic energies in the case of Xe projectiles seem to be consistent with both models. Furthermore, the mean number of atoms per ejected cluster is dependent on the projectile ion. This is clearly in contrast to our statements on process ii). Thus, at least the Xe^{44+} data with the larger $\bar{n}$ value should be significantly influenced by process iii) and the corresponding sticking probability seems to be reasonable. By noting that $\bar{n}$ is per definition larger than one, we find that the value that we predict for Cs projectiles on the basis of Eq. (5) for process iii) is significantly lower than the corresponding experimental value. Hence, for Cs there seems to be a dominant contribution due to process ii) as stated also in the work of Abdullaeva et al. [32]. From Eq. (5) we may estimate that the total sputtering yield has to exceed 1.5 for process iii) to be dominant. Thus, it is no surprise that Abdullaeva et al. did not find any indication for the statistical off-surface mechanism iii), since all data have been taken for singly charged low-energy ions at energies far below the nuclear stopping power maximum.

Fig. 4 displays experimental mass distributions of $Si_nO_mH_l$ compounds sputtered off a quartz surface that is grown from a silicon wafer in dry air. The negative-cluster fractions are plotted as a function of the projectile charge state q for O^{7+}-, Xe^{27+}-, Xe^{44+}- and U^{67+}-ions at energies of about 2.6 keV/amu. The sum over the cluster fractions is normalized to one for each incident charge state. It is noted, that a surface cleaning was performed with a conventional Ar-sputtering gun before each measurement in order to achieve reproducable surface conditions (similar hydrogen contaminations). At $q = -1$ results for desorption by 2-keV electron impact are also displayed [16]. In that investigation mass spectra were taken only up to $M = 50$ amu and no information on heavier clusters is given. However, a comparison of the SiO^+ intensity for 2-keV electrons [16] and 2.2-keV/amu Xe^{30+}-ions [20] indicates that heavier clusters play a minor role in case of electron impact.

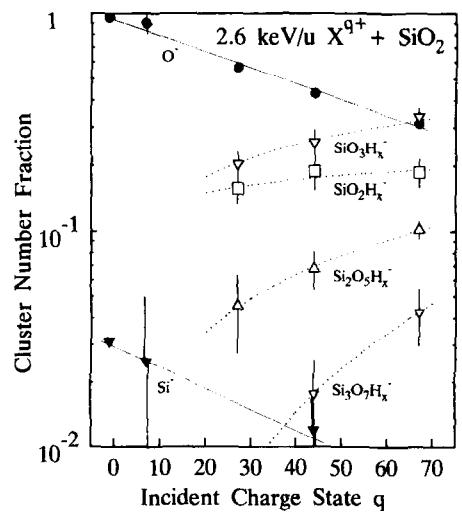

Fig. 4. Negative-cluster fractions $Si_nO_mH_l^-$ plotted as a function of the projectile charge state q for O^{7+}-, Xe^{27+}-, Xe^{44+}- and U^{67+}-ions at energies of about 2.6 keV/amu. The 2-keV electron results are taken from Ref. [16].

From Fig. 4 it is evident that the $Si_nO_mH_l$ cluster distribution is charge-state dependent. Any possible projectile-mass dependence seems to be of minor importance, as can be seen from the significant differences between the results for Xe^{27+}- and Xe^{44+}-ions. We observe that only monomers are significantly sputtered for charge states below 10. Furthermore, we find that the mean number of atoms (O and Si) in a negative cluster increases to $\bar{n} = 3.5 \pm 0.5$ for U^{67+}-ions. According to the above discussion of the carbon data this is a clear signature for a statistical off-surface production mechanism and the corresponding average sticking probabilities are on the order of 0.5. Thus, for high charge states the production of $Si_nO_mH_l$ clusters appears similar as in the carbon case. But in contrast to the carbon data there is no indication for sputtering-as-an-entity in the case of low charge states (low sputtering yields).

4. Summary

The single-detector technique introduced in this work allows for very efficient negative-ion time-of-flight measurements on an absolute intensity scale in the case of highly charged ions and it should be applicable for a broad range of incident energies. Measurements of this type may also be used for a non-destructive surface analysis, as a total of only 10^7 ions with "currents" on the order of 1000 ions per second are sufficient to yield the spectra shown in this work. Further improvements of the sensitivity are expected if such measurements are performed under nearly-grazing-incidence conditions [3].

In conclusion, this work has opened some possibilities and it has shown future perspectives to investigate basic sputtering mechanisms in the case of highly-charged heavy ions as well as the formation of clusters at surfaces. The investigation of carbon sputtering gave some evidence for the sputtering-as-an-entity concept of cluster formation in the case of low total sputtering yields [32]. Furthermore, an influence of thermal spikes could be excluded for the light targets investigated in this work. For large total sputtering yields, however, we favour a statistical off-surface cluster-production mechanism. For the SiO_2 target the clusters seem to be produced only via such statistical processes.

One challenging task for a better quantitative understanding of the processes involved in sputtering of clusters is left open, however. That is the determination of the positive, negative and *neutral fractions* for each cluster size, especially *for high incident charge states*. For U^{67+}-ions, e.g., the nuclear stopping power is enhanced by about a factor of 3 compared to singly charged U ions, but electronic sputtering rates might be enhanced by up to a factor 5000. Thus, as soon as electronic processes are involved, it is necessary to perform experiments with a variety of ions with different incident charge states.

Acknowledgements

The authors would like to thank D.A. Knapp for providing us with his data acquisition system as well as D. DeWitt and D. Nelson for their help during the preparation of the experiment. We would also like to express our gratitude to H.H. Andersen for his help in improving the introduction and discussion sections of this paper. To a large extend this work was supported by NATO grant GRG920075. Part of this work was performed under the auspices of U.S. Dept. of Energy by the Lawrence Livermore National Laboratory under contract W-7405-ENG-48.

References

[1] W.R. Grove, Philos. Mag. 5 (1853) 203.
[2] G. Granquist, Ofvers. Svenska Vet. Akad. Forh. 54 (1897) 575; ibid. 55 (1898) 709.
[3] H.H. Andersen and H.L. Bay, Sputtering by Particle Bombardment, ed. R. Behrisch (Springer, Berlin, Heidelberg, New York, 1982) p. 145.
[4] W.L. Brown, Mat. Res. Soc. Symp. Proc. 51 (1985) 53.
[5] R.P. Edwin, J. Phys. D 6 (1973) 833.
[6] R.A. Dugdale and S.D. Ford, Trans. Br. Ceram. Soc. 65 (1966) 165.
[7] B.N. Makarenko, A.B. Popov, A.A. Shaporenko and A.P. Shergin, Radiat. Eff. Defects in Solids 113 (1990) 263.
[8] B. Emmoth and M. Braun, Phys. Scripta 24 (1981) 415.
[9] J.P. Biersack and W. Eckstein, Appl. Phys. A 34 (1984) 73.
[10] M.W. Thompson, Philos. Mag. 18 (1968) 377.
[11] P. Sigmund, Sputtering by Particle Bombardment, ed. R. Behrisch (Springer, Berlin, Heidelberg, New York, 1982) p. 9.
[12] P. Sigmund, Phys. Rev. 184 (2) (1969) 383; Nucl. Instr. and Meth. B 27 (1987) 1.
[13] H.M. Urbassek, Interaction of charged particles with solids and surfaces, eds. A. Gras-Marti, H.M. Urbassek, N.R. Arista and F. Flores NATO ASI series B: Physics Vol. 271 (1991) p. 227.
[14] H.H. Andersen and H.L. Bay, J. Appl. Phys. 46 (1975) 2416; H.L. Bay, H.H. Andersen, W.O. Hofer and O. Nielsen, Nucl. Instr. and Meth. 132 (1976) 301; H.H. Andersen, K. Dan. Vidensk. Selsk. Mat. Fys. Medd. 43 (1993) 127.
[15] T. Diaz de la Rubia, Radiat. Eff. Defects in Solids 130/131, in press (1994).
[16] R.A. Baragiola and T.E. Madey, Interaction of Charged Particles with Solids, eds. A. Gras-Marti, H.M. Urbassek, N. Arista and F. Flores, (NATO ASI series B: Physics Vol. 271 Plenum, New York, 1991) p. 313; A.-M. Lanzillotto, T.E. Madey and R.A. Baragiola, Phys. Rev. Lett. 67 (1991) 232.
[17] E.S. Parilis, Proc. Int. Conf. on Atomic Collision Phenomena in Solids, Amsterdam (1970) p. 324; I.S. Bitenskii, M.N. Murakhmetov and E.S. Parilis, Sov. Phys.-Tech. Phys. 24 (1979) 618.
[18] T.Y. Arifov, D.D. Gruich and S.N. Morozov, Proc. 5th All-Union Conf. on the Interaction of Atomic Particles with Solids, Minsk (1987) Vol.1, p. 200.

[19] S.T. de Zwart, T. Fried, D.O. Boerma, R. Hoekstra, A.G. Drentje and A.L. Boers, Surf. Sci. 177 (1986) L939.
[20] G. Schiwietz, D. Schneider, M. Clark, B. Skogvall, D. DeWitt and J. McDonald, Radiat. Eff. Defects in Solids 127 (1993) 11.
[21] H.H. Andersen, Vacuum 39 (1989) 1095.
[22] R.E. Marrs, M.A. Levine, D.A. Knapp and J.R. Henderson, Phys. Rev. Lett. 60 (1988) 1715;
D.H. Schneider, M. Clark, B.M. Penetrante, J. McDonald, D. DeWitt and J.N. Bardsley, Phys. Rev. A 44 (1991) 3119.
[23] H. Kurz, K. Töglhofer, H.P. Winter, F. Aumayr and R. Mann, Phys. Rev. Lett. 69 (1992) 1140;
F. Aumayr, H. Kurz, D. Schneider, M.A. Briere, J.W. McDonald, C.E. Cunningham and H.P. Winter, Phys. Rev. Lett. 71 (1993) 1943.
[24] G. Schiwietz, J.P. Biersack, D. Schneider, N. Stolterfoht, D. Fink, V.J. Montemayor and B. Skogvall, Phys. Rev. B 41 (1990) 6262;
D. Schneider, G. Schiwietz and D. DeWitt, Phys. Rev. A 47 (1993) 3945.
[25] B. Skogvall and G. Schiwietz, Phys. Rev. A 46 (1992) 5687.
[26] R.D. DuBois, Phys. Rev. A 36 (1987) 2585;
R.D. DuBois and A. Kövèr, Phys. Rev. A 40 (1989) 3605.
[27] W. Begemann, K.H. Meiwes-Broer and H.O. Lutz, Phys. Rev. Lett. 56 (1986) 2248.
[28] R.E. Honig, J. Chem. Phys. 22 (1954) 126.
[29] M.Y. Hahn, E.C. Honea, A.J. Paguia, K.E. Schriver, A.M. Camarena and R.L. Whetten, Chem. Phys. Lett. 130 (1986) 12.
[30] K.S. Pitzer and E. Clementi, J. Am. Chem. Soc. 81 (1959) 4477.
[31] S. Yang, K.J. Taylor, M.J. Craycraft, J. Conceicao, C.L. Pettiette, O. Cheshnovsky and R.E. Smallay, Chem. Phys. Lett. 144 (1988) 431.
[32] M.K. Abdullaeva, B.G. Atabaev and R. Dzabbarganov, Nucl. Instr. and Meth. B 62 (1991) 43.
[33] D. Teillet-Billy and J.P. Gauyacq, Surf. Sci. 239 (1990) 343.
[34] P.J. Jennings, R.O. Jones and M. Weinert, Phys. Rev. B 37 (1988) 6113.
[35] J.K. Norskov and B.I. Lundquist, Phys. Rev. B 19 (1979) 5661.
[36] G.P. Können, A.P. Tip and A. de Vries, Radiat. Eff. 21 (1974) 269; ibid. 26 (1975) 23.